Joint Channel Estimation and Equalization Using Circular Convolution and DNN for ZP-OTFS

Feng-Yu Chang, Min-Che Hsieh, and Chia-Han Lee

***Abstract*—To combat the Doppler shift caused by high mobility, orthogonal time frequency space (OTFS) systems have been proposed to convert the time-varying channel into a nearly time-invariant channel in the delay-Doppler (DD) domain. Since the DD domain received signal can be expressed as a two-dimensional (2D) circular convolution of the transmitted signal and the channel impulse response in the DD domain, we propose a joint channel estimation and equalization method based on 2D circular convolution, called circular convolution based joint channel estimation and equalization (C-JCE), for zero-padding (ZP) OTFS systems. However, when the Doppler shift is severe and the subcarrier spacing is not large enough, the phase distortion may occur. As a result, we further propose a deep learning (DL)-based method, called pilot-aided phase distortion compensation network (PDCN), to compensate the phase distortion. The proposed C-JCE with PDCN achieves a bit error rate performance close to the minimum mean square error (MMSE) or message passing (MP) equalization with perfect channel state information (CSI) on the low earth orbit (LEO) satellite channel with an extremely large Doppler shift. Overall, the proposed C-JCE with PDCN for ZP-OTFS systems not only has a higher spectral efficiency but also achieves an outstanding performance.**

***Index Terms*—OTFS, deep learning, LEO, channel estimation, equalization, 2D circular convolution.**

I. Introduction

To achieve the global coverage of communication services, the low earth orbit (LEO) satellite communication (SATCOM) is critical for next generation communication systems. However, LEO satellites have high mobility due to the low altitude, which leads to high Doppler shifts. Orthogonal time frequency space (OTFS), a modulation scheme which transmits the data symbols via the delay-Doppler (DD) domain, transforms a time-varying multi-path channel into a nearly time-invariant channel [1], [2], [3] and thus becomes popular for LEO satellite communications [4]. Nevertheless, a sufficient subcarrier spacing is required to keep the DD domain channel nearly time-invariant, leading to low spectral efficiency.

Various channel estimation schemes have been designed for OTFS systems. Raviteja *et al.* propose an embedded pilot (EP)-based method which puts pilots and guard symbols in the DD domain frame to estimate the channel impulse response [5]. Ramachandran and Chockalingam [6] and Hashimoto *et al.* [7] propose to place pilots in a frame separate from the frame for data symbols. However, since they assume that the frame for channel estimation and the frame for data symbols pass through the same channel, their methods may not be effective when the estimated channel is outdated in the next frame. In a work by Murali and Chockalingam [8], the channel estimation is performed in the time-frequency (TF) domain. To allow for more data symbols to be transmitted, the schemes proposed by Mishra *et al.* [9] and Yuan *et al.* [10] make the pilots superimposed to the data symbols. In addition, a sparse Bayesian learning-based channel estimation has been proposed by Zhao *et al.* [11]. Furthermore, Shen *et al.* propose a three dimensional (3D)-structured orthogonal matching pursuit algorithm for channel estimation [12]. Although the aforementioned methods have better performance and higher spectral efficiency than the EP-based methods, they incur higher complexity. In terms of equalization, several methods have been proposed for OTFS systems. A message passing (MP) algorithm has been proposed by Raviteja *et al.* [2], but their method causes high complexity. To solve that, Thaj and Viterbo propose a low complexity iterative decision feedback equalization (DFE) based on maximal ratio combining (MRC) which achieves better bit error rate (BER) performance than the MP detector with lower complexity [13]. The linear equalizations such as zero-forcing (ZF) detection and minimum mean square error (MMSE) detection have also been discussed [3], [14]. Recently, deep learning (DL) has been applied for signal detection in OTFS systems, showing promising performances [15]. However, these methods assume perfect channel state information (CSI) which are impractical and the performance may degrade due to imperfect channel estimation. Furthermore, Hashimoto *et al.* [7] propose a 2D deconvolution method to equalize the received signals for cyclic prefix (CP)-OTFS systems. However, their method uses two frames for channel estimation and equalization, resulting in low spectral efficiency.

In this paper, we propose a joint channel estimation and equalization method for zero-padding (ZP)-OTFS systems [3], [16] based on the EP-based channel estimation and the 2D circular convolution equalization, called circular convolution based joint channel estimation and equalization (C-JCE). ZP-OTFS is adopted due to its potentially higher spectral efficiency than CP-OTFS systems [3]. Nevertheless, if the 2D deconvolution equalization is directly applied to the LEO SATCOM channels with large Doppler shifts, the phase distortion may

F.-Y. Chang, M.-C. Hsieh, and C.-H. Lee are with Institute of Communications Engineering, National Yang Ming Chiao Tung University, Hsinchu, Taiwan (e-mail: chiahan@nycu.edu.tw). This work is supported in part by the National Science and Technology Council (NSTC), Taiwan under grants 110-2221-E-A49-022-MY3, 112-2221-E-A49-078-MY3, and 113-2218-E-A49-027.

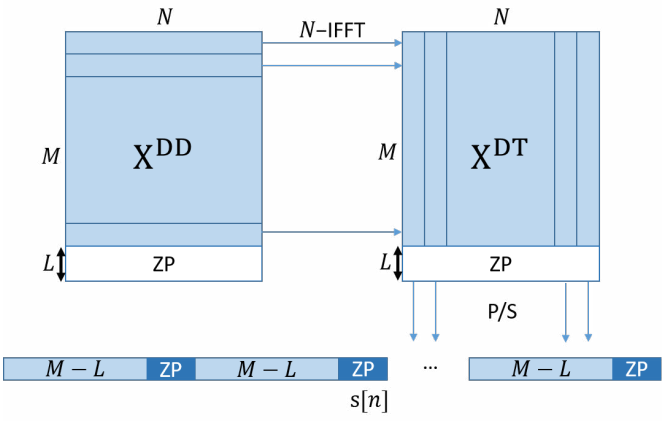

(a) Modulation

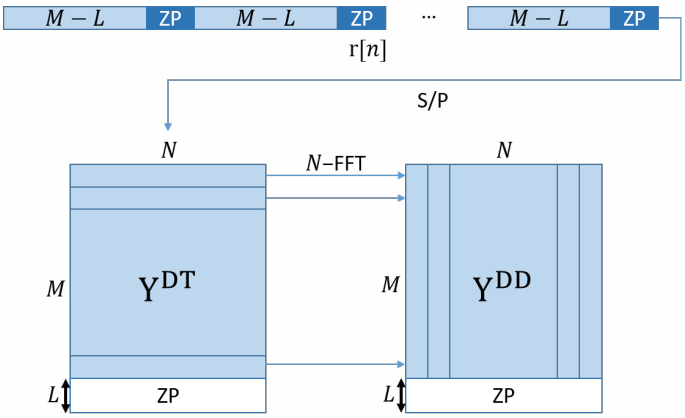

(b) Demodulation

Fig. 1: ZP-OTFS

occur since the channel may no longer be nearly time-invariant in the DD domain. Therefore, we propose to use deep neural networks to compensate the phase distortion. The proposed pilot-aided phase distortion compensation network (PDCN) improves the BER performance significantly, allowing the proposed C-JCE with PDCN to approach the performance of MMSE or MP equalization with perfect channel estimation even when the Doppler shift is extremely large.

II. System Model

The ZP-OTFS moduation is shown in Fig. 1(a). Consider that $\mathrm{X}^{\mathrm{DD}}[m,n]$, $m=0,\ldots,M-1, n=0,\ldots,N-1$, is a DD domain grid with size $M\times N$ for data symbol transmission. L_{ZP} denotes the length of the ZP which should be larger or equal to $l_{\max}$, the maximum path delay. Different from CP, ZP is placed on the DD domain grid X^{DD}. Then, X^{DD} is transformed into the delay-time (DT) domain grid X^{DT} by performing inverse fast Fourier transform (IFFT) on each row. Finally, X^{DT} is reshaped into a sequence and sent to the receiver. At the receiver, the OTFS demodulation is conducted to regenerate the DD domain signal X^{DD}, as shown in Fig. 1(b). Different from CP, ZP will not be removed. While performing equalization, the ZP will be equalized with data symbols.

TABLE I: The NTN-TDL-D channel model.

Path No.	Avg. Power (dB)	Delay	Fading Distribution
1	-0.284	0	LOS path
	-11.991	0	Rayleigh
2	-9.887	0.5596	Rayleigh
3	-16.771	7.3340	Rayleigh

In LEO SATCOM systems, the Doppler shift f_d can be calculated by $f_d = f_{d,\mathrm{LEO}}+(v_{\mathrm{t}}/c)(f_c+f_{d,\mathrm{LEO}})\cos\theta$, where v_{t}, c, f_c, and θ are respectively the terminal velocity, the light speed, the carrier frequency, and a random variable uniformly distributed between 0 and 2π satisfying Jake's spectrum [17]. $f_{d,\mathrm{LEO}}$ is the Doppler shift due to the movement of LEO satellites, which can be expressed as $f_{d,\mathrm{LEO}} = (v_{\mathrm{sat}}/c)(\frac{R}{R+h}\cos\alpha_{\mathrm{sat}})f_c$, where v_{sat}, R, h, and α_{sat} denote the satellite speed, the earth radius, the satellite altitude, and the satellite elevation angle, respectively.

We consider the 3GPP NTN-TDL-D channel model [17] with the power delay profile shown in TABLE I—the first tap has a line-of-sight (LOS) part following the Rician distribution and the rest two taps are none-line-of-sight (NLOS) following the Rayleigh distribution. The delay spread values of the TDL model is then scaled by the desired delay spread. In this paper, the desired delay spread is set such that the delay spread equal or smaller than $(L_{\mathrm{ZP}}-1)/2$.

III. Proposed Joint Channel Estimation and Equalization for ZP-OTFS

A. Proposed C-JCE

The proposed joint channel estimation and equalization for ZP-OTFS, i.e., C-JCE, adopts the EP-based channel estimation. The symbol arrangement of the proposed C-JCE is shown in Fig. 2. The guard interval is put at the bottom of the frame, and the pilot is put at the far-left column. The guard interval between the pilot and the bottom, along with the guard interval between the data symbols and the pilot, should be larger or equal to the maximum delay $l_{\max}$ in the delay domain so that the received data symbols do not pollute the interval for channel estimation. Since the guard interval between the pilot and the bottom is larger or equal to $l_{\max}$, it satisfies the condition of ZP so that it can also be a ZP of the frame. In addition, since the guard interval between the data symbols and the pilot is larger or equal to $l_{\max}$, it also satisfies the condition of ZP. Hence, the grids inside the green dash line which consist of data symbols and a part of ZP can be regarded as a ZP-OTFS frame by itself.

At the receiver, the received DD domain signal Y^{DD} can be expressed as the circular convolution of X^{DD} and the DD domain channel impulse response as $\mathrm{Y}^{\mathrm{DD}} = \mathrm{X}^{\mathrm{DD}} \circledast \Lambda$, where $\circledast$ and Λ respectively denote the 2D circular convolution operation and the estimated DD domain channel impulse response. Note that Hashimoto *et al.* [7] utilize this property to propose using 2D deconvolution [18] to equalize the received signal in CP-OTFS systems. However, they use two frames for channel estimation and

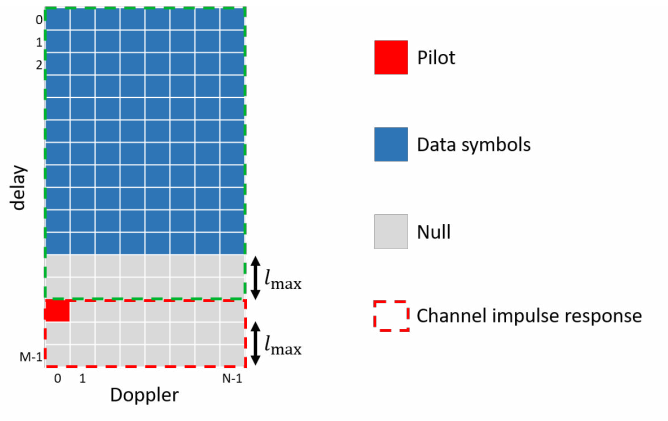

Fig. 2: An example of the proposed transmission frame.

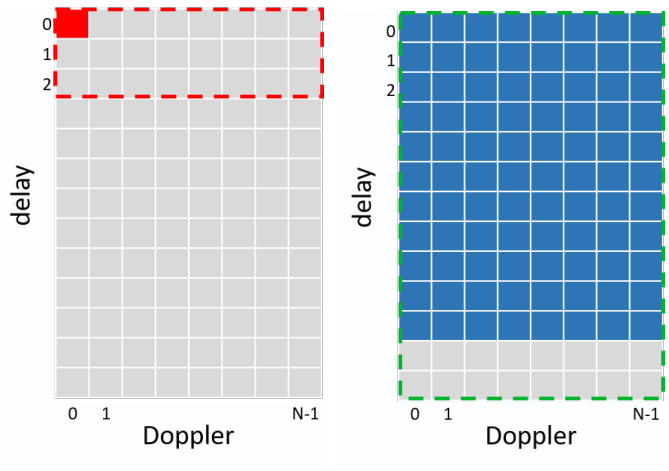

(a) $\tilde{\Lambda}$ (b) $\tilde{\mathrm{Y}}^{\mathrm{DD}}$

Fig. 3: Illustration of $\tilde{\Lambda}$ and $\tilde{\mathrm{Y}}^{\mathrm{DD}}$.

equalization which is inefficient in terms of spectral efficiency. On the contrary, the ZP-OTFS system considered here allows for better spectral efficiency than CP-OTFS. Leveraging the above observations, the proposed C-JCE for ZP-OTFS combines the EP-based channel estimation and the 2D deconvolution equalization. Since the grids inside the green dash line in Fig. 2 can be regarded as a ZP-OTFS frame by itself, we use the estimated channel impulse response (through the grids inside the red dash line) to equalize the received symbols in the grids inside the green dash line. Let $\tilde{\mathrm{Y}}^{\mathrm{DD}}$ denote the received symbols on grids inside the green dash line and let Λ' be the channel impulse response estimated from the grids inside the red dash line in Fig. 2. Firstly, zero padding is performed to Λ' such that the resulting $\tilde{\Lambda}$, as shown in Fig. 3(a), has the same size with $\tilde{\mathrm{Y}}^{\mathrm{DD}}$ in Fig. 3(b). Then, the 2D Wiener deconvolution is performed as [18]

$$\mathcal{F}\left(\hat{\mathrm{X}}^{\mathrm{DD}}\right)[m,n] = \frac{\mathcal{F}(\tilde{\Lambda})^*[m,n]}{|\mathcal{F}(\tilde{\Lambda})[m,n]|^2+\sigma^2}\mathcal{F}\left(\tilde{\mathrm{Y}}^{\mathrm{DD}}\right)[m,n], \tag{1}$$

where $\hat{\mathrm{X}}^{\mathrm{DD}}$, $\mathcal{F}(\cdot)$, $(\cdot)^*$, and σ^2 respectively denote the equalized symbols on grids inside the green dash, the 2D discrete Fourier transform (DFT), the conjugate operation, and the noise variance. $\hat{\mathrm{X}}^{\mathrm{DD}}$ is then obtained by $\hat{\mathrm{X}}^{\mathrm{DD}}[m,n] = \mathcal{F}^{-1}(\mathcal{F}(\hat{\mathrm{X}}^{\mathrm{DD}}))[m,n]$, where $\mathcal{F}^{-1}(\cdot)$ is 2D IDFT. Finally, we remove the ZP to obtain the data.

B. Proposed PDCN for Phase Distortion Compensation

If the subcarrier spacing is not large enough, the channel in the DD domain is no longer nearly time-invariant and the channel impulse response may not be estimated accurately. The equalized symbols may then suffer from the phase distortion. Note that the channel impulse response only varies in the delay domain, and the variation of the channel impulse response is only on the phase. Accordingly, we propose PDCN, which uses pilots and deep neural networks, to compensate the phase distortion. An example of the pilot placement is shown in Fig. 4. The pilots for the phase distortion compensation are placed in every two lattices of column 1 and column 2 at the interval for data symbol transmission (i.e., the purple grids). The pilot power is set equal to the power of data symbols. After equalization, the grids inside the purple dash line in Fig. 4 are extracted as an input of PDCN to compensate the phase distortion. The PDCN layers are given in TABLE II. Note that batch normalization is performed between the 2D convolution (Conv2D) layer and the activation function, and B denotes batch size.

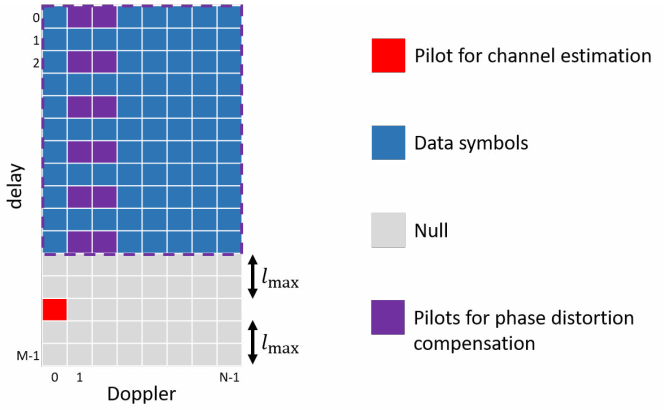

Fig. 4: An example of pilots for phase distortion compensation.

TABLE II: Layers of the proposed PDCN.

Layer	Filter Size	Kernel Size	Activation Function	Output Dimension
Input	-	-	-	$(B, M, N, 2)$
Conv2D	32	5	PReLU	$(B, M, N, 32)$
Conv2D	16	5	PReLU	$(B, M, N, 16)$
Conv2D	16	3	PReLU	$(B, M, N, 16)$
Conv2D	8	3	PReLU	$(B, M, N, 8)$
Conv2D	8	3	PReLU	$(B, M, N, 8)$
Conv2D	2	3	tanh	$(B, M, N, 2)$
Output	-	-	-	(B, M, N)

TABLE III: Simulation parameters.

Parameter	Value
M	64
N	16
CP and ZP length, L_{CP}, L_{ZP}	7
Modulation	QPSK
SNR of pilot for channel estimation	50 dB
Satellite height	1500 km
Minimum elevation angle	50°
Maximum terminal velocity	500 km/h

IV. Performance Evaluation

The setup in TABLE III is used for performance evaluation. The pilots are placed at $1, 5, \ldots, 1+4i, \ldots, 57$ of the 4th and 5th columns, and $3, 7, \ldots, 3+4i, \ldots, 55$ of the 12th and 13th columns, $i \in \mathbb{N}$. We choose 10 ns as the desired delay spread when the subcarrier spacing is 480 KHz and 30 ns otherwise. The DL training parameters are the following. There are 150000 training samples, the batch size is 32, the optimizer is Adam with 0.0001 learning rate, the loss function is mean squared error, the training SNR is 20 dB, and the number of epochs is 100. The training and simulations are performed on a desktop computer equipped with Intel Core i7-11700 @ 2.50 GHz, 32G DRAM, and NVIDIA GeForce RTX 3060 GPU.

First of all, let us compare the spectral efficiency of ZP- and CP-OTFS systems. Denoting L_{CP} as the CP length and Q as the modulation order, the spectral efficiency of the considered ZP-OTFS is calculated as $\frac{M-L_{\mathrm{ZP}}}{M}\log_2 Q = 1.78$ while that of the CP-OTFS by Hashimoto *et al.* [7] is $\frac{M}{2(M+L_{\mathrm{CP}})}\log_2 Q = 0.9$. It can be seen that the considered ZP-OTFS system has higher spectral efficiency.

In the simulations, the proposed C-JCE and C-JCE+PDCN are compared with Hashimoto *et al.* [7] with perfect channel estimation and the EP-based channel estimation with MMSE or MP equalization. Various carrier frequencies and subcarrier spacing are considered since the Doppler shift is proportional to the carrier frequency and inversely proportional to the subcarrier spacing. As shown in Fig. 5(a), with the 4 GHz carrier frequency and the 480 KHz subcarrier spacing, C-JCE, the proposed /C-JCE+PDCN and the comparing schemes all perform very well, approaching the performance using the perfect channel estimation + MMSE or MP equalization. However, when the subcarrier spacing decreases to 240 KHz, C-JCE and the scheme by Hashimoto *et al.* [7] both degrade significantly, as shown in Fig. 5(b). If the subcarrier spacing is further decreased to 120 KHz, the EP-based methods begin to degrade, especially when the MP equalization is performed, as shown in Fig. 5(c). On the contrary, the proposed C-JCE+PDCN performs very well, approaching the performance of perfectly-known channel with MMSE/MP equalization, even when the subcarrier spacing is only 120 KHz.

When the carrier frequency is increased to 10 GHz, as shown in Fig. 6, C-JCE, the scheme by Hashimoto *et al.* [7], and EP + MP do not perform well when the subcarrier spacing is 480 KHz or smaller, and EP + MMSE begins to degrade significantly when the subcarrier spacing becomes 240 KHz. Again, only the proposed C-JCE+PDCN performs well throughout all subcarrier spacing scenarios. Finally, we keep increasing the carrier frequency to 20 GHz. As shown in Fig. 7, only the proposed C-JCE+PDCN works even when the subcarrier spacing is 480 KHz. When the subcarrier spacing is down to 120 KHz with the Doppler shift being extremely large, the proposed C-JCE+PDCN still has decent performance.

TABLE IV: Computational complexity.

Methods	FLOPs
Hashimoto *et al.* [7]	1.97×10^5
EP + MMSE	1.07×10^9
C-JCE	1.97×10^5
Proposed C-JCE + PDCN	3.46×10^7

The complexities of the proposed C-JCE+PDCN and the comparing methods are shown in TABLE IV. Although the complexity of the proposed C-JCE+PDCN is higher than the method by Hashimoto *et al.* [7], the complexity is much lower than EP + MMSE.

V. Conclusions

In this paper, we have proposed a novel joint channel estimation and equalization method for ZP-OTFS and a deep neural network to compensate the phase distortion caused by the insufficient subcarrier spacing. The proposed C-JCE+PDCN not only has higher spectral efficiency but also delivers outstanding performance under the LEO SATCOM channel with large Doppler shift due to the small subcarrier spacing. In particular, the performance of the proposed C-JCE+PDCN approaches the perfect CSI MMSE or MP equalization under various scenarios.

References

[1] R. Hadani, S. Rakib, M. Tsatsanis, A. Monk, A. J. Goldsmith, A. F. Molisch, and R. Calderbank, "Orthogonal time frequency space modulation," in *Proc. IEEE Wireless Communications and Networking Conference (WCNC)*, 2017, pp. 1–6.

[2] P. Raviteja, K. T. Phan, Y. Hong, and E. Viterbo, "Interference cancellation and iterative detection for orthogonal time frequency space modulation," *IEEE Transactions on Wireless Communications*, vol. 17, no. 10, pp. 6501–6515, 2018.

[3] Y. Hong, T. Thaj, and E. Viterbo, *Delay-Doppler Communications: Principles and Applications*. Elsevier, 2022.

[4] X. Wang, W. Shen, C. Xing, J. An, and L. Hanzo, "Joint Bayesian channel estimation and data detection for OTFS systems in LEO satellite communications," *IEEE Transactions on Communications*, vol. 70, no. 7, pp. 4386–4399, 2022.

[5] P. Raviteja, K. T. Phan, and Y. Hong, "Embedded pilot-aided channel estimation for OTFS in delay–Doppler channels," *IEEE Transactions on Vehicular Technology*, vol. 68, no. 5, pp. 4906–4917, 2019.

[6] M. Kollengode Ramachandran and A. Chockalingam, "MIMO-OTFS in high-Doppler fading channels: Signal detection and channel estimation," in *Proc. IEEE Global Communications Conference (GLOBECOM)*, 2018, pp. 206–212.

[7] N. Hashimoto, N. Osawa, K. Yamazaki, and S. Ibi, "Channel estimation and equalization for CP-OFDM-based OTFS in fractional Doppler channels," in *Proc. IEEE International Conference on Communications Workshops (ICC Workshops)*, 2021, pp. 1–7.

[8] K. R. Murali and A. Chockalingam, "On OTFS modulation for high-Doppler fading channels," in *Proc. Information Theory and Applications Workshop (ITA)*, 2018, pp. 1–10.

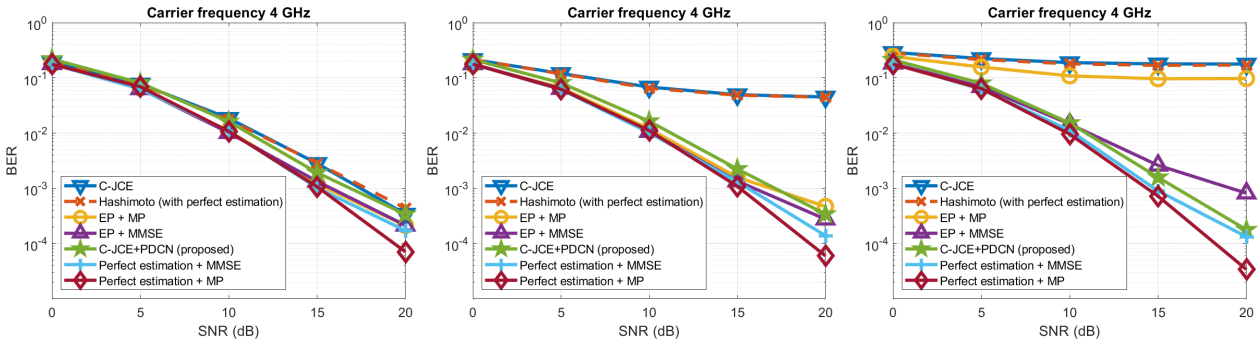

(a) 480 KHz subcarrier spacing (b) 240 KHz subcarrier spacing (c) 120 KHz subcarrier spacing

Fig. 5: Performance with 4 GHz carrier frequency.

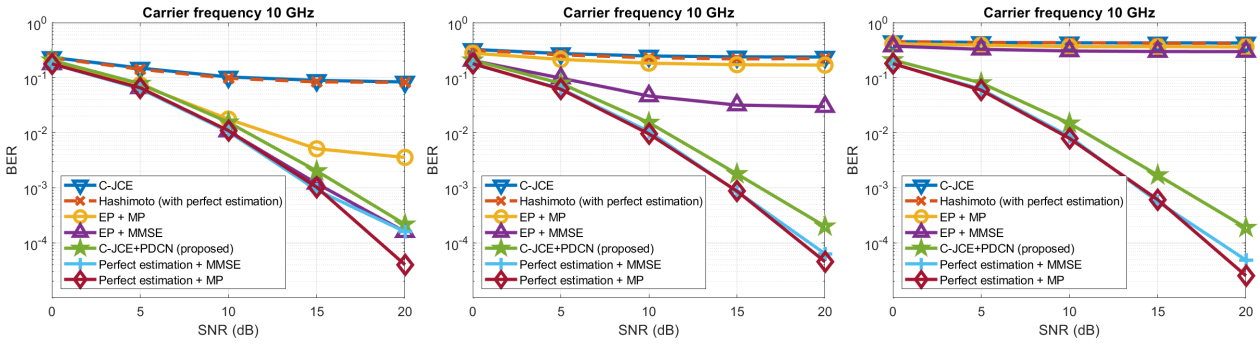

(a) 480 KHz subcarrier spacing (b) 240 KHz subcarrier spacing (c) 120 KHz subcarrier spacing

Fig. 6: Performance with 10 GHz carrier frequency.

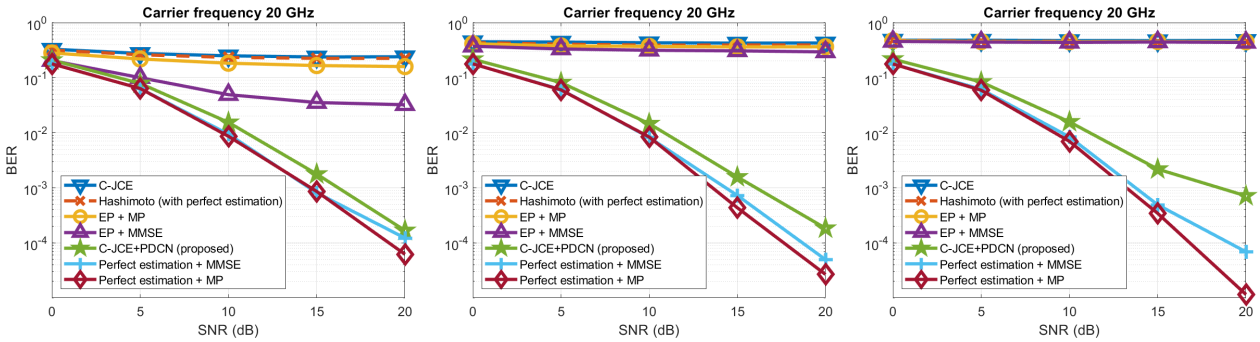

(a) 480 KHz subcarrier spacing (b) 240 KHz subcarrier spacing (c) 120 KHz subcarrier spacing

Fig. 7: Performance with 20 GHz carrier frequency.

[9] H. B. Mishra, P. Singh, A. K. Prasad, and R. Budhiraja, "OTFS channel estimation and data detection designs with superimposed pilots," *IEEE Transactions on Wireless Communications*, vol. 21, no. 4, pp. 2258–2274, 2022.

[10] W. Yuan, S. Li, Z. Wei, J. Yuan, and D. W. K. Ng, "Data-aided channel estimation for OTFS systems with a superimposed pilot and data transmission scheme," *IEEE Wireless Communications Letters*, vol. 10, no. 9, pp. 1954–1958, 2021.

[11] L. Zhao, W.-J. Gao, and W. Guo, "Sparse Bayesian learning of delay-Doppler channel for OTFS system," *IEEE Communications Letters*, vol. 24, no. 12, pp. 2766–2769, 2020.

[12] W. Shen, L. Dai, J. An, P. Fan, and R. W. Heath, "Channel estimation for orthogonal time frequency space (OTFS) massive MIMO," *IEEE Transactions on Signal Processing*, vol. 67, no. 16, pp. 4204–4217, 2019.

[13] T. Thaj and E. Viterbo, "Low complexity iterative Rake decision feedback equalizer for zero-padded OTFS systems," *IEEE Transactions on Vehicular Technology*, vol. 69, no. 12, pp. 15 606–15 622, 2020.

[14] P. Singh, A. Gupta, H. B. Mishra, and R. Budhiraja, "Low-complexity ZF/MMSE MIMO-OTFS receivers for high-speed vehicular communication," *IEEE Open Journal of the Communications Society*, vol. 3, pp. 209–227, 2022.

[15] Z. Zhou, L. Liu, J. Xu, and R. Calderbank, "Learning to equalize OTFS," *IEEE Transactions on Wireless Communications*, vol. 21, no. 9, pp. 7723–7736, 2022.

[16] T. Thaj, E. Viterbo, and Y. Hong, "General I/O relations and low-complexity universal MRC detection for all OTFS variants," *IEEE Access*, vol. 10, pp. 96 026–96 037, 2022.

[17] "3rd Generation Partnership Project; Technical Specification Group Radio Access Network; Study on New Radio NR to Support Non-terrestrial Networks (Release 15)," 3GPP, Tech. Rep. TR 38.811 V15.4.0, 2020.

[18] G. Dougherty and Z. Kawaf, "The point spread function revisited: image restoration using 2-D deconvolution," *Radiography*, vol. 7, pp. 255–262, 2001.